Overview of Improved Confinement and Plasma Control in the MST Reversed Field Pinch

J.S. Sarff 1), A.F. Almagri 1), J.K. Anderson 1), T.M. Biewer 1), A.P. Blair 1), D.L. Brower 2), M.D. Carter 3), M. Cengher 1), B.E. Chapman 1), P.K. Chattopadhyay 1), V.I. Davydenko 6), D.J. Den Hartog 1), W.X. Ding 2), F. Ebrahimi 1), G. Fiksel 1), C.B. Forest 1), J.A. Goetz 1), R.W. Harvey 4), D. Holly 1), B. Hudson 1), A.A. Ivanov 6), T.W. Lovell 1), K.J. McCollam 1), P.D. Nonn 1), R. O'Connell 1), S.P. Oliva 1), R.I. Pinsker 5), S.C. Prager 1), J.C. Reardon 1), S.D. Terry 1), M.A. Thomas 1), M.D. Wyman 1), C. Xiao 7), and the MST Team 1)

1) University of Wisconsin-Madison, Madison, WI 53706 USA
2) Electrical Engineering Department, University of California, Los Angeles, California USA
3) Oak Ridge National Laboratory, Oak Ridge, Tennessee USA
4) CompX, Del Mar, California USA
5) General Atomic, LaJolla, California USA
6) Budker Institute of Nuclear Physics, Novosibirsk Russia
7) University of Saskatchewan, Saskatoon, Saskatchewan Canada

email contact: jssarff@wisc.edu

Abstract. Energy confinement comparable to tokamak quality is achieved in the MST reversed field pinch at high beta and relatively low magnetic field. Magnetic fluctuations normally present in the RFP are reduced via parallel current drive in the outer region of the plasma. In response, the electron temperature nearly triples and beta doubles. The confinement time increases ten-fold (to ~10 ms), which is comparable to L- and H-mode scaling values for a tokamak with the same plasma current, density, heating power, shape and size. Fast electron confinement is evidenced by hard x-ray bremmstrahlung. Fokker-Planck modeling requires the electron diffusivity be velocity-independent to reproduce the x-ray energy flux, implying the residual transport is not magnetic stochasticity in origin. To extend profile control and add auxiliary heating, rf current drive and neutral beam heating are in development. Low power rf systems are installed to examine lower-hyrbrid wave injection ($\leq$ 12 kW from a stripline antenna) and electron Bernstein wave injection ($\leq$ 120 kW from a waveguide antenna). DC current sustainment via AC helicity injection (sinusoidal inductive loop voltages) is also being tested. Low power neutral beam injection shows fast ions are well-confined, even with relatively large magnetic fluctuations present.

1. Introduction

The reversed-field pinch (RFP) configuration represents toroidal fusion plasma confinement in the limit where the magnetic field is small and strongly sheared. In particular, the toroidal magnetic field applied at the plasma boundary is typically ~ 100 times smaller than for a tokamak with the same plasma current. The potential benefits of a fusion reactor core based on the RFP include high beta (and very high "engineering beta"), high power density, small forces on normal-conducting magnet coils, simple assembly, and the possibility for Ohmic ignition [1]. Demonstration of fusion-relevant plasma confinement in a relatively weak magnetic field has been the principal challenge for RFP research. In this paper we report the confinement of T_e >1 keV plasmas with an electron heat transport conductivity χ_e ~5-10 m^2/s in the MST RFP, comparable to the heat transport rate of tokamak plasmas with a magnetic field strength 10 times larger at the plasma surface.

Large radial transport from parallel streaming in a stochastic magnetic field must be avoided in any fusion plasma. Toroidal configurations with strong external magnetization tend not to suffer this problem. This is not the case for the standard RFP, which is unstable to resistive MHD tearing and relies on a fluctuation-induced emf (e.g., the MHD dynamo $\langle \tilde{\mathbf{V}} \times \tilde{\mathbf{B}} \rangle$) to sustain essential poloidal current flowing in the outer region of the plasma. The standard RFP fusion development path depends on a large reduction of the dynamo's constituent tearing fluctuations as the plasma's electrical resistivity decreases. The scaling of these fluctuations is subject to resistive MHD physics and is not very favorable to date [2,3]. One hope is that the dynamo emf could be obtained with a single, large instability, avoiding multiple island formation and widespread magnetic stochasticity that normally occurs. Such a "single-helicity" dynamo has been observed in MHD computation [4,5], with hints in experimental plasmas that it might be stimulated to occur under controllable conditions [6].

A different RFP fusion development path based on external current drive to maintain a stable current profile has emerged in recent years. This requires the addition of poloidal current drive for improved plasma stability, or equivalently, for the replacement of the dynamo emf present in standard RFP sustainment. The current profile is maintained directly, rather than relying on dynamo to redistribute current within the plasma. The improved RFP confinement conditions described in this paper were obtained using time-dependent inductive electric field programming, a technique referred to as pulsed poloidal (or parallel) current drive (PPCD) [7,8,9,10]. A programmed ramp of the toroidal field winding current is used to generate poloidal induction. Current drive based on RF techniques is in development for MST.

When PPCD programming is applied to MST plasmas, magnetic fluctuations decrease and confinement improves. The core electron temperature increases nearly three-fold while the Ohmic input power *decreases*, unambiguous evidence of reduced electron heat transport. The substantial temperature gradient usually confined to a narrow edge region in standard RFP plasmas extends into the core during PPCD. Fast electrons become confined, evidenced by a ~ 100-fold increase in hard x-ray bremsstrahlung emission. Fokker-Planck modeling reveals that the diffusion of these electrons does not depend on their parallel velocity and is no longer characteristically magnetic in origin. The global energy confinement time increases 10-fold to a value comparable to L- and H-mode expectations for a tokamak of the same current, density, size, and shape.

In the following sections we describe these confinement-related results in more detail, along with progress in quantitative understanding of energy transport in a stochastic magnetic field. We also describe progress in developing plasma control tools for MST using RF current drive and heating, neutral beam heating, and Oscillating Field Current Drive.

2. Tokamak-like Energy Confinement in MST

The Madison Symmetric Torus (MST) is a circular cross-section torus with dimensions R = 1.5 m and a = 0.5 m (large for RFP experiments) and toroidal current $I_\phi \leq 0.5$ MA [11]. Standard fueling is deuterium. The inductive current drive programming for PPCD is illustrated in Fig. 1. The toroidal, E_ϕ , and poloidal, E_θ , electric fields (from loop voltages) applied at the plasma surface are shown in Fig. 1(a). The essential ingredient for PPCD is $E_\theta > 0$, accomplished with circuitry that ramps the toroidal field winding current in time. As a byproduct, the edge toroidal field, $B_\phi(a)$, and safety factor, $q = rB_\phi / RB_\theta$, become more negative during this time. The parallel inductive electric field, $E_\parallel = (E_\phi B_\phi + E_\theta B_\theta)/B$, is

shown in Fig. 1(b) to emphasize the desired goal $E_{||} > 0$ for direct sustainment of current in the outer region of the plasma. Typical reduction of magnetic fluctuations measured at the plasma surface is shown in Fig. 1(c). The fluctuations are primarily from global MHD tearing with mode numbers $m = 1$, $n \geq 6$ resonant throughout the core and $m = 0$, $n \geq 1$ resonant at the $q = 0$ surface near the edge of the plasma. Stochastic transport associated with these modes is discussed in section 4 below.

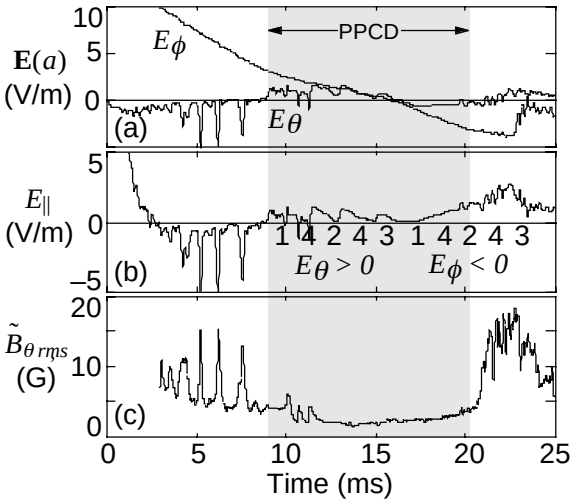

FIG 1. (a) Toroidal and poloidal inductive electric field, (b) parallel electric field, and (c) rms (poloidal) magnetic fluctuation at r = a for PPCD.

In standard RFP operation, E_ϕ is held constant to maintain a stationary toroidal current, while $E_\theta \approx 0$ (stationary toroidal flux except near strong dynamo events, appearing as negative E_θ spikes). Hence $E_{||} < 0$ at the boundary of standard RFP plasmas, tending to peak and de-stabilize the current profile. To extend PPCD, E_ϕ is instead allowed to decrease and reverse sign as shown in Fig. 1(a). Since $B_\phi(a) < 0$, reversed $E_\phi < 0$ maintains $E_{||} > 0$. This is effective near the end of the toroidal field ramp when $B_\phi(a)$ is most negative. The combination of loop voltages in Fig. 1 produces the longest and most complete fluctuation reduction to date [9,12]. However, PPCD programming is inherently transient, always terminating in a non-disruptive loss of improved confinement conditions as the fluctuation amplitude increases.

Temperature Profiles and Local Heat Transport

The electron temperature increases dramatically when magnetic fluctuations are reduced. The $T_e(r)$ profiles for 400 kA standard and PPCD-improved plasmas are compared in Fig. 2(a), obtained with a movable, single-point Thomson scattering diagnostic at $t = 18$ ms (near the end of PPCD in Fig. 1). The line average density is 1.0×10^{19} m^{-3} in both cases. The radial resolution in these profiles is the maximum acquired to date for MST, with each data point representing an average measurement for ~ 5 similar plasmas. These profiles therefore represent average PPCD-improved performance. Construction of $T_e(r)$ with less radial resolution but using only the best PPCD plasmas (lowest fluctuation amplitudes) shows similar core temperatures but larger T_e in the outer region of the plasma. A maximum $T_e(0) = 1.2$ keV has been measured in high quality 500 kA PPCD plasmas [12].

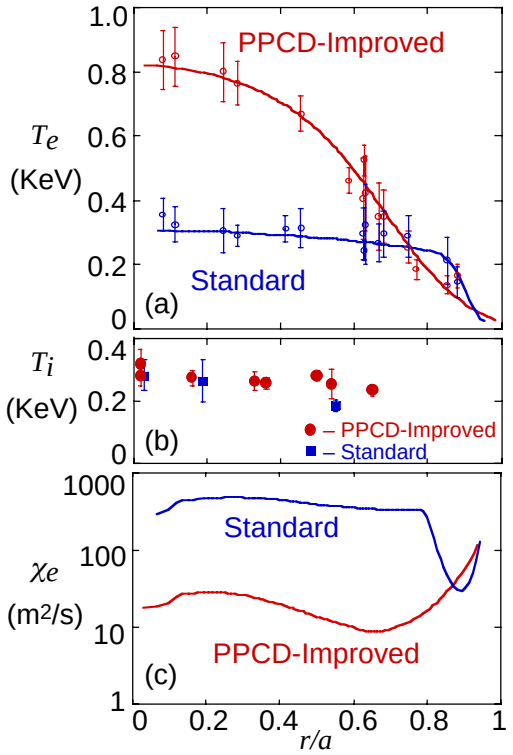

FIG. 2. Radial profiles of (a) electron temperature, (b) C^{+6} ion temperature, and (c) electron heat conductivity. Global τ_E increases 5-fold in this case.

Unlike the electron temperature, the ion temperature does not change significantly, shown in Fig. 2(b) for both standard and PPCD plasmas. These profiles are the C^{+6} impurity temperature measured by charge exchange recombination spectroscopy (along a diagnostic neutral beam). The majority ion temperature measured by Rutherford scattering of a neutral beam is similar to the impurity ion temperature. The ions in standard plasmas are heated by a poorly understood mechanism correlated with magnetic reconnection and dynamo [13], but classical collisional heating may be sufficient in improved confinement plasmas. Ion energy transport analysis is difficult when an anomalous heating mechanism is involved. This remains a topic of active research.

Improved electron energy confinement is self-evident in Fig. 2(a): the temperature increases—which *decreases* the Ohmic heating power—and the temperature gradient extends well into the core during PPCD. Local transport analysis confirms this result. A novel toroidal equilibrium reconstruction approach [14] provides direct measurement of the local Ohmic heating power density $\mathbf{E} \cdot \mathbf{J}$, avoiding uncertainties in evaluating the plasma resistivity, mostly due to difficulty in the measurement of Z_{eff}. (The measurement of Z_{eff} is most accurate for PPCD plasma conditions, with good agreement between $\mathbf{E} \cdot \mathbf{J}$ and ηJ^2.) The equilibrium reconstructions are constrained by 11 chords of FIR polarimetry [15], an on-axis measure of the magnetic field using the motional Stark effect [16], as well as conventional edge magnetic measurements.

The electron heat conductivity profiles, $\chi_e(r)$, for standard and PPCD-improved plasmas are compared in Fig. 2(c). Losses associated with electron-ion collisions, radiation, and thermal convection are subtracted from the input power to isolate the conducted heat flux $q_e = -\chi_e n \nabla T_e$. A dramatic decrease in χ_e is evident across the plasma radius during PPCD, and the global energy confinement time increases to $\tau_E \approx 5$ ms, a five-fold improvement relative to standard plasmas. Selecting the best PPCD plasmas, the global confinement improvement is estimated to be ten-fold to $\tau_E \approx 10$ ms, with minimum $\chi_e \sim 5$ m^2/s [9].

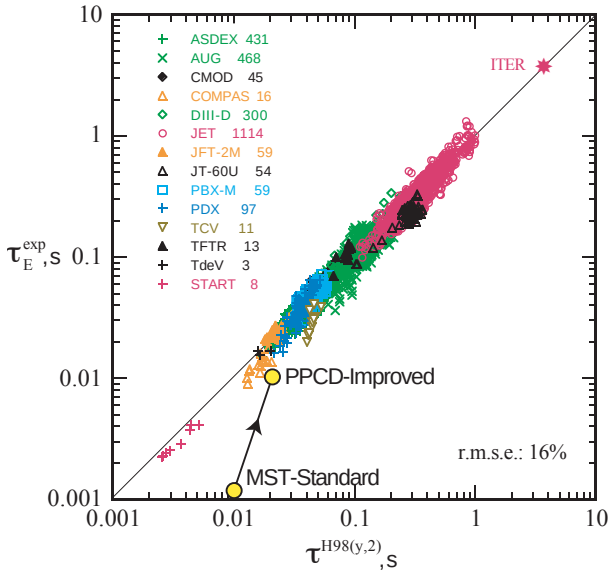

FIG 3. MST confinement relative to tokamak H-mode empirical scaling. (Reprinted from ITER Physics Guidelines, ITER report N 19 FDR 1 01-07-13 R 0.1.)

Comparison with Tokamak Confinement via Empirical Scaling

The heat conductivity $\chi_e \sim 5$ m^2/s observed during PPCD is comparable to that in tokamak plasmas, therefore the global confinement time should be comparable as well. There is no unique way to compare global confinement in different toroidal magnetic geometries, especially when a major configuration knob is substantially different, in this case the toroidal magnetic field strength. A comparison using the IPB98(y,2) ELMy H-mode tokamak empirical scaling is shown in Fig. 3. The tokamak data comes from the ITER physics database used to construct scaling formulae [17]. The data point labeled "PPCD-Improved" is

τ_E = 10 ms for I_ϕ = 200 kA PPCD plasmas plotted against the tokamak scaling-projected value τ_E = 23 ms derived from the IPB98(y,2) engineering parameter formula calculated with MST's current, density $n = 0.7 \times 10^{19}$ m^{-3}, (Ohmic) input power P = 0.5 MW, major radius, aspect ratio, and circular-shape (κ = 1). The point labeled "MST-Standard" is standard RFP confinement $\tau_E \approx 1$ ms compared the same way. The IPB98(y,2) scaling's toroidal field sensitivity~ $B^{0.15}$ is weak, so the value chosen matters little (an interesting fact in this comparison), but B = 1.0 T corresponds to typical tokamak operation with q_a = 4. For reference, the L-mode scaling-projected confinement time is τ_E = 18 ms, and the neo-Alcator (Ohmic) scaling-projected confinement time is τ_E = 31 ms for this same q_a = 4 "equivalent" tokamak using similar empirical formulas [17]. Note that the poloidal gyro-radius is the same for tokamak and RFP plasmas if the plasma current and temperature are the same.

This comparison shows that PPCD-improved global RFP confinement is indeed comparable to confinement expectations for a tokamak, but with the important difference that $B_\phi(a)$ is 20 times smaller in the MST RFP than for the q_a = 4 "equivalent" tokamak ($B_\phi(a) \approx 0.05$ T for 200 kA PPCD). The total field strength at the plasma surface—including the dominant poloidal field—is 10 times smaller than the equivalent tokamak. It should be emphasized that the similarity of confinement times in this comparison does *not* imply tokamak scaling applies to PPCD-improved RFP plasmas. Too little data exist to draw conclusions regarding the scaling of an RFP with minimized MHD tearing fluctuations, which could be much different than tokamak scalings.

Beta Improvement

The increase in electron temperature during PPCD leads to a doubling of beta [9]. Maximum beta is achieved in 200 kA plasmas, where the total beta, $\beta_{tot} = \langle p \rangle / B^2(a)$, increases from 9% in standard plasmas to 15% during PPCD. Poloidal beta $\beta_\theta = \langle p \rangle / B_\theta^2(a) \approx \beta_{tot}$ in standard plasmas since $B_\theta(a) \approx B(a)$. Because inductive poloidal current drive increases $|B_\phi(a)|$, $\beta_\theta \approx 18\%$ is a little larger than $\beta_{tot} \approx 15\%$ during PPCD. In higher current 400 kA plasmas the beta enhancement factor is larger, with β_{tot} increasing from 5% to 11%. Hence the beta reduction observed with increasing current in standard plasmas is substantially lessened with PPCD. Toroidal beta $\beta_\phi = \langle p \rangle / B_\phi^2(a)$, as commonly defined for tokamak and ST experiments, is less relevant for an RFP since the vacuum toroidal field is small ($\beta_\phi \to \infty$ by letting $q_a \to 0$). During PPCD, toroidal beta decreases to $\beta_\phi \approx 80\%$ since $|B_\phi(a)|$ increases.

Beta is high in the RFP, but generally about a factor of two less than the ideal MHD limit defined by interchange stability. The theoretical pressure profile which satisfies the Suydam (or Mercier) criterion at all radii defines an ideal beta limit $\beta_\theta \approx 20\%$ for MST's standard equilibrium, increasing to $\beta_\theta \approx 30\%$ during PPCD from increased magnetic shear. The measured pressure gradients are close to the theoretical ideal interchange limit in the edge and core where magnetic shear is weakest, but there is no obvious phenomenon that limits the pressure. The beta limiting physics in the RFP is unknown, and is more likely associated with resistive MHD, e.g., pressure-driven tearing, or g-modes which are always unstable (but with small linear growth rates when $\beta << 1$).

3. Confinement of Fast Electrons

Collisionless diffusion in a stochastic magnetic field scales as ~ $v_\parallel D_m$, where $v_\parallel$ is the parallel particle velocity and D_m is the magnetic field line diffusivity. The distribution of high energy

electrons is therefore a sensitive indicator of magnetic surface quality. A ~ 100-fold increase in hard x-ray bremsstrahlung emission during PPCD implies the confinement of fast electrons is vastly improved. The x-ray energy flux spectra for standard and PPCD plasmas are shown in Fig. 4, measured using a solid state CdZnTe detector. The absence of photons with energy >20 keV in standard plasmas shows that electrons of similar energy are not confined. In contrast, electrons >100 keV are present during PPCD.

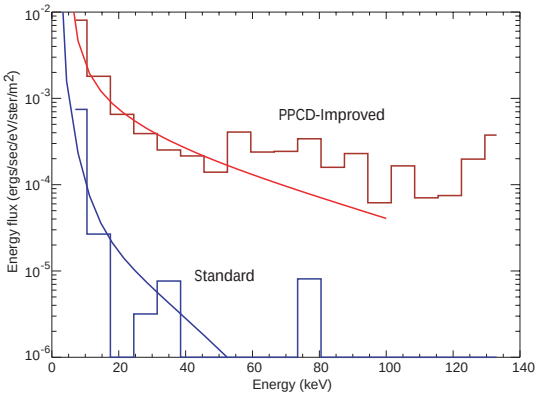

FIG. 4. Hard x-ray energy flux spectra. Smooth curves are fits from Fokker-Plank modeling.

Fokker-Planck transport modeling has been used to reconstruct the x-ray flux, thereby inferring the diffusive properties of the collisionless electrons [18]. The multi-species, toroidal, relativistic Fokker-Planck code CQL3D [19] evolves the ion and electron distributions in a Maxwellian background defined by the measured density and temperature profiles. The calculated bremmstrahlung from ion-electron collisions is compared with the measured x-ray flux, and the radial diffusion coefficient is adjusted to match the x-ray emission and, simultaneously, the measured parallel electric field and current density profiles from equilibrium reconstruction.

The smooth lines overlaying the binned experimental data in Fig. 4 are the best-fit Fokker-Planck reconstructions of the x-ray flux. To achieve reasonable fits, the parallel velocity dependence in the particle diffusion coefficient for standard plasmas is $D \sim v_{\|e}$, characteristic of transport in a stochastic magnetic field, but for the PPCD case D is independent of velocity, suggesting stochastic-loss is no longer dominant. Velocity-independent D is more characteristic of electrostatic turbulent transport like that observed in tokamak and stellarator plasmas.

4. Heat Transport in a Stochastic Magnetic Field

Although collisionless particle and energy transport in a stochastic magnetic field is fundamentally non-local, the process of field line diffusion requires local tearing and reconnection at many radii to form an extended region of magnetic stochasticity. The measured safety-factor profile, $q(r)$, for typical standard plasma conditions in MST is shown in Fig. 5(a), determined by toroidal equilibrium reconstruction. The large magnetic shear associated with $q \rightarrow 0$ permits many low-mode-number rational surfaces on which magnetic islands can form. The close spacing of these surfaces renders the magnetic field susceptible to island overlap, especially near the $q = 0$ toroidal field reversal surface. The dominant magnetic fluctuations observed in the RFP are global $m = 1$, $n > q(0)^{-1} \approx 5$ tearing modes resonant inside the reversal surface, as well as $m = 0$ modes resonant at the reversal surface. The typical island widths associated with the $m = 1$, $n \leq 15$ modes are superposed on the $q(r)$ profile in Fig. 5(a). A toroidal array of 32 magnetic sensors measures the amplitudes of these modes at the plasma surface in MST.

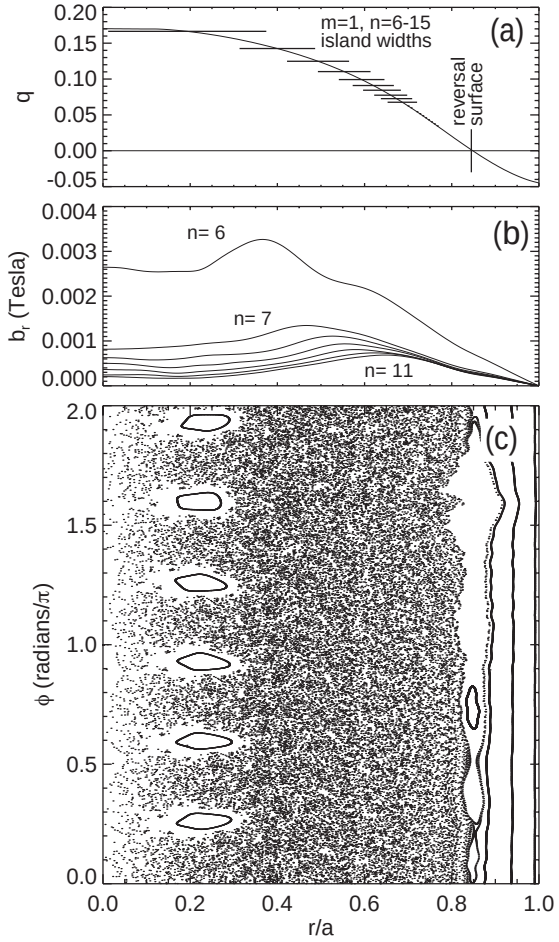

FIG. 5. (a) Standard RFP q(r), (b) profiles of core-resonant m=1 radial magnetic fluctuations, and (c) field line tracing puncture plot in toroidal plane.

A magnetic field line tracing code is used to visualize and quantify the magnetic stochasticity resultant from the dominant magnetic fluctuations in MST standard plasmas [20]. The mean-field profiles are input from the experimental equilibrium reconstruction, while the fluctuating-field profiles are input from 3D (cylindrical), nonlinear, resistive MHD computation using the DEBS code [21]. Such computation has long been used for theoretical investigation of the MHD dynamo process that occurs in standard RFP plasmas, reproducing experimental fluctuation characteristics and dynamo behavior remarkably well. To model MST plasmas, the nonlinear computation is performed at effective aspect ratio $R/a = 3$ and Lundquist number $S \approx 10^6$, very close to the experimental value $S \approx 3 \times 10^6$ for the ~ 400 kA case described here. The profiles of the computed radial magnetic fluctuation, $\tilde{b}_{rn}(r)$, are shown in Fig. 5(b) for the dominant $m = 1$ modes, normalized by matching the transverse field fluctuation amplitudes measured at the plasma surface. A thick conducting shell surrounds MST plasmas (and in the computation), forcing $b_r(a) \rightarrow 0$. To model possible stochasticity out to the reversal surface, mode numbers $n \leq 32$ are included in the field line tracing code. The amplitudes of modes $16 \geq n \geq 32$ are extrapolated from the measured spectrum $n \leq 15$.

The field line tracing puncture plot shown in Fig. 5(c) for the toroidal plane illustrates the widespread magnetic stochasticity expected in the core of standard RFP plasmas. Island structure is evident only for the inner-most mode $m = 1$, $n = 6$ and for $m = 0$ modes at the reversal surface. The non-stochastic boundary outside the reversal surface may not be accurate since modes resonant in this region have not been included in the field line tracing. However, $b_r(a) \rightarrow 0$ dictates that well-formed surfaces must exist near the plasma boundary, likely somewhat thinner radially than indicated in Fig. 5(c).

The magnetic diffusivity can be calculated directly from field line tracing by forming the ensemble average $D_m = \langle \Delta r^2 / \Delta L \rangle$ for the field line radial excursion Δr over the field line length ΔL. The predicted heat conductivity for stochastic magnetic transport $\chi_e = v_{Te} D_m$ is compared with the measured χ_e in Fig. 6(a), agreeing surprisingly well. The field line tracing reproduces large $\chi_e \sim 500$ m^2/s in the core, as well as the relative transport barrier $\chi_e \sim 50$ m^2/s near the reversal surface. Although the line tracing may not be accurate near the reversal surface, measured $\chi_e \sim 50$ m^2/s is consistent with the measured global energy

confinement time of $\tau_E \approx 1$ ms. The reversal surface is unique because all $m = 0$ modes are resonant at the same location and the magnitude of $\tilde{b}_{rn}$ is relatively small compared to $m = 1$ modes, both from close proximity to the conducting shell at $r = a$, and from the longer wavelength of $m = 0$, $n \sim 1$ modes. The magnetic transport associated with $m = 0$ modes should be smaller as a result. More $m = 1$ modes need to be included in the field line tracing to resolve the region surrounding the reversal surface.

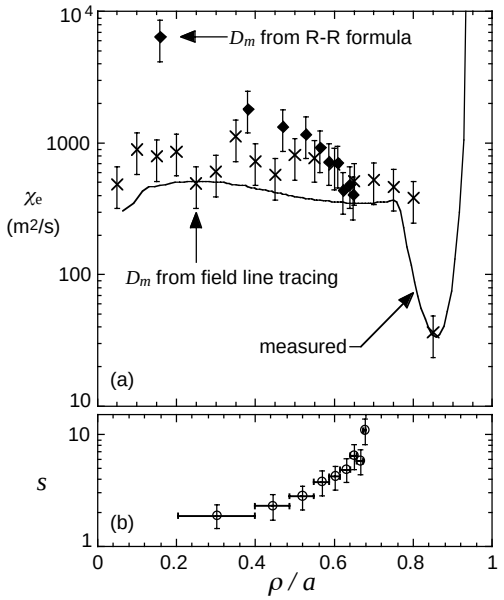

FIG. 6. (a) Calculated stochastic magnetic conductivity $\chi_e = v_{Te} D_m$ compared to measured χ_e and (b) Chirikov island overlap paramter versus radius.

The often-used estimate $\chi_e^{RR} = v_{Te} \pi L_{eff} \tilde{b}_{rn}^2 / B^2$ derived by Rechester-Rosenbluth [22] is shown in Fig. 6(a) for $n \leq 15$. In contrast to direct field line tracing, the R-R estimate agrees with the measured χ_e only in the region where the resonant surface density is highest, just inside the reversal surface. The Chirikov parameter $s = (w_{mn} + w_{m'n'})/2(r_{mn} - r_{m'n'})$ is shown in Fig. 6(b), which measures the overlap of adjacent islands of width w_{mn} located at resonant surfaces r_{mn}. An accurate estimate using the Rechester-Rosenbluth formulation appears to require $s > 5$. Note that although the mode amplitudes are largest in the core, the islands are weakly overlapped there ($s \sim 1$), yielding much less catastrophic heat conductivity than estimated by χ_e^{RR}.

Role of the Mode Spectrum for Improved RFP Confinement

The localized nature of resonant field line tearing is well-illustrated in the standard RFP. Many adjacent resonant modes of significant amplitude are required to move field lines across the radius of the plasma. It thus becomes clear that to reduce stochastic magnetic transport in the RFP requires broadband mode suppression, especially the high-n, $m = 1$ modes resonant inside the reversal surface.

The PPCD-induced fluctuation reduction shown in Fig. 1(c) is the total spectral rms, dominated by the largest mode $n = 6$. The reduction of high-n modes is typically much greater. The maximum $T_e(0)$ achieved during PPCD—a good single-indicator of energy confinement in an Ohmically heated plasma—occurs when the time-average amplitude of high-n modes is smallest. This is shown in Fig. 7(a), where $T_e(0)$ near the end of PPCD ($t = 18$ ms in Fig. 1) is plotted against the rms fluctuation amplitude $\sqrt{\sum_n b_{\theta n}^2(a)}$ for $8 \leq n \leq 15$, time-averaged from the start-to-end of PPCD ($t = 12$-18 ms in Fig. 1). The data points labeled "+" are measurements from individual plasmas with the same density and identical PPCD programming. The fluctuation reduction varies somewhat shot-to-shot, revealing an excellent correlation of higher $T_e(0)$ with sustained low amplitudes of high-n modes. The data point labeled "Standard" is the average $T_e(0)$ and high-n rms mode amplitude for steady-state standard plasmas (same current and density). To maximize the database of shots available for this analysis, a double-filter (Be) soft x-ray measurement of the core electron temperature is used, calibrated to Thomson scattering measurements of the core temperature T_e ($r/a < 0.2$) obtained in a subset of the shot database.

A similar correlation of $T_e(0)$ and magnetic fluctuation amplitude is shown in Fig. 7(b), but for the single $m = 1$, $n = 6$ mode resonant closest to the magnetic axis in the same shots as for Fig. 7(a). The $n = 6$ is the largest mode in the spectrum in the vast majority of MST plasmas, sometimes *increasing* in magnitude during PPCD. (The adjacent $n = 7$ mode is rarely larger.) Two striking features are revealed in Fig. 7(b). First, the correlation between $T_e(0)$ and the dominant—and therefore total—fluctuation amplitude is weak. Second, the temperature in the core is weakly influenced by the nearest resonant mode. Both features are understandable considering the discussion above for magnetic transport in RFP plasmas. The core temperature is being supported by low heat conductivity in the mid-radius region where many high-n modes are resonant (see $\chi_e(r)$ in Fig. 2). A large mode resonant in the core weakly impacts global confinement. Transport within an isolated island may be large, but not beyond its outer radius. This is analogous to the weak impact of $m = 1$, $n = 1$ sawtoothing on tokamak confinement when the $q = 1$ surface remains close to the magnetic axis.

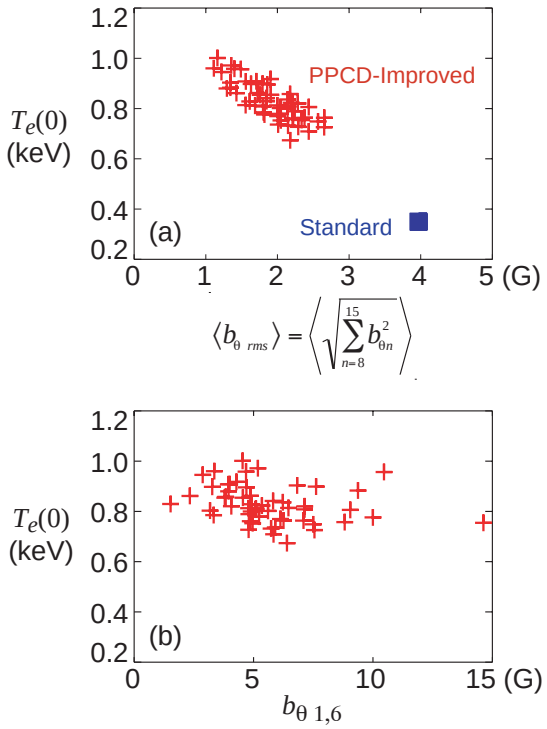

FIG. 7. (a) Core electron temperature versus time-average rms fluctuation amplitude of $8 \le n \le 15$ modes. (b) Core electron temperature versus amplitude of the dominant mode m=1, n=6.

5. Other Plasma Control Tools

Transient inductive current drive has become a very effective tool for magnetic fluctuation and transport control in the RFP. Although PPCD-like inductive current drive could be attractive in a pulsed-reactor scenario, non-transient rf techniques have potential for more precise and localized profile control. Lower-hybrid and electron Bernstein wave (EBW) scenarios are being tested at low power in MST. AC helicity injection, sometimes called Oscillating Field Current Drive (OFCD), is being tested for steady-state inductive current sustainment and possibly profile control. In addition to current drive, either rf scenario would provide auxiliary heating as well. The more direct approach using neutral beam injection is also being evaluated. No substantial auxiliary heating has been used in RFP research to date, partly because Ohmic heating has always been large. Since beta and confinement are coupled in Ohmically heated plasma, auxiliary heating would permit direct investigation of the unknown beta-limiting phenomena in the RFP.

A second-generation interdigital-line antenna is installed in MST for launching 800 MHz, $n_{\|} \sim 8$ lower hybrid (LH) waves. The power limit continues to increase with antenna conditioning, up to ~12 kW with low ~ 10% reflection. Probe instrumentation measures an e-folding length ~ 9 cm of the damped power along the antenna, a little less than two wavelengths $\lambda_{LH} = 4.8$ cm. This damping length continues to increase with antenna

conditoning, with proper spectrum control for current drive requiring ~ 3-4λ_{LH}. The relatively small-area feedthrough for this antenna may be the principal reason for the observed power limit in this and the first-generation antenna. Small feedthrough port size is one of the attractive features of the interdigital-line approach, well suited to MST. However, sufficient power must be achieved for a tractable high power experiment with multiple antennas.

The observation of thermal levels of electron cyclotron emission suggests, by reciprocity, that EBW current drive and heating can be done in the overdense RFP [23]. A twin waveguide antenna has been installed on a 11.4 cm port to launch 3.1-3.8 GHz waves in MST. Two traveling-wave tubes provide ≤120 kW power launched with minimum ~ 10% reflection. At low power, the amplitude of the reflected power varies with the relative phasing of the two waveguides, in qualitative agreement with theoretical analysis of coupling. Moreover the coupling is best during PPCD, bolstering the viability of EBW current profile control. The obtained 120 kW is ~ 10% of the Ohmic heating power during PPCD, so RF heating might be an observable perturbation in temperature-related measurements. A search for absorption signatures in soft and hard x-ray emission is presently underway.

Current sustainment in the RFP is especially difficult, given that the pressure-driven neoclassical bootstrap current is small. A long-standing hope for the RFP is AC helicity injection using low frequency sinusoidal modulation of the inductive loop voltages, sometimes called Oscillating Field Current Drive (OFCD). Bevir and Gray [24] recognized that $\pi/2$ relative phasing of the loop voltages injects time-average DC magnetic helicity to maintain a DC plasma current (with small AC modulation) if the plasma maintains a relaxed-state. Two ~ 500 Hz, < 1 MVA oscillators have been installed in MST's Ohmic circuits to test partial current drive by OFCD. First results are shown in Fig. 8. The additional current provided by low-power OFCD is small (as expected). The dependence on the relative phase of the oscillators agrees very well with helicity injection expectations, reproducing a key result from the first (and only other) OFCD experiment in ZT-40M [25]. New 3D, nonlinear, resistive MHD computation at high Lundquist number demonstrates sustainment of DC plasma current with sinusoidal loop voltages, forming a theoretical basis to evaluate and optimize OFCD experiments in MST [26]. A key issue to be explored is compatibility with confinement, since OFCD is based on relaxation physics which operates in standard RFP plasmas.

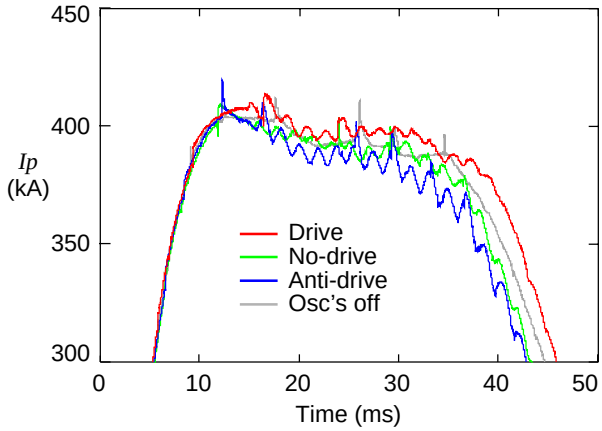

FIG. 8. Toroidal plasma current with OFCD oscillators phased for current drive ("Drive"), anti-current drive ("Anti-drive"), and no current drive ("No-drive"). These should be compared to oscillators turned off ("Osc's off").

A low-current (diagnostic) neutral beam [27] has been used for the first exploration of fast ion confinement in the RFP. Figure 9 shows measured fast charge-exchange neutrals observed following the abrupt shut-off of the neutral beam in standard RFP plasmas. In the two cases shown, 1 ampere equivalent H neutrals were injected at 10 kV and 20 kV perpendicular to the plasma along a central chord. The slow decay of the fast ion background greatly exceeds not only the bulk particle confinement time ~ 1 ms but also the loss time expected for stochastic magnetic diffusion ~$v_{\|} D_m$, with D_m inferred from χ_e measurements in

the core (Fig. 6). The loss rate is identical for both 10 kV and 20 kV injected neutrals, also uncharacteristic of stochastic diffusion. Finite gyroradius averaging could explain why fast ions are more weakly affected by magnetic stochasticity than fast electrons in standard RFP plasmas. A short pulse, ~ 1 MW beam is being tested as the next step toward high power neutral beam heating. Fast ion confinement will be examined in greater detail for tangential beam injection.

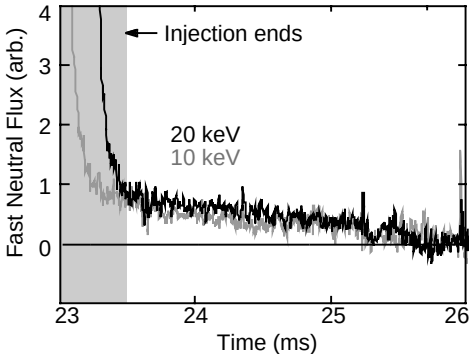

FIG. 9. Fast neutral background following abrupt neutral beam turn-off. By design, the charge exchange flux is large while the beam is on. Neutral signal following the beam is indicative of confined fast ions.

6. Summary

Energy confinement similar to tokamak quality has been obtained in the MST reversed field pinch at high beta and relatively low magnetic field. Magnetic fluctuations, which cause widespread magnetic stochasticity in the core of standard RFP plasmas, are reduced by inductive current drive targeted to the edge region of the plasma. Fast electrons > 100 keV are confined, and Fokker-Planck modeling infers that the diffusion of these high energy electrons is independent of velocity, therefore not magnetic in nature and more like electrostatic-turbulent transport seen in tokamak and stellarator plasmas. In contrast, the heat diffusivity in standard plasmas agrees well with stochastic transport expectations. The importance of high-n modes resonant inside the $q = 0$ surface is revealed in the strong correlation of high core temperature with low $m = 1$, $n \geq 8$ mode amplitudes. The global energy confinement improves 10-fold to a value comparable to an equivalent tokamak of the same current, density, heating power, size and shape, but with 20 times smaller applied toroidal field in the MST RFP.

The inductive techniques used to create improved confinement in MST are inherently transient. To sustain and refine current profile control, non-inductive current drive using rf techniques are in development. Lower-hybrid and electron Bernstein wave injection experiments are underway at low power. If successful, the rf techniques could provide auxiliary heating as well as localized current drive. Good fast ion confinement revealed through diagnostic neutral beam injection suggests efficient neutral beam heating might be possible as well. High power, short pulse beam injection experiments are beginning. Lastly, current sustainment by AC helicity injection (or Oscillating Field Current Drive) is being tested. Fractional current drive in accordance with helicity balance predictions is observed with installed low power oscillators.

References

[1] NAJMABADI, F., CONN, R.W. et al., *The TITAN Reversed Field Pinch Reactor Study—The Final Report*, UCLA Report UCLA-PPG-1200 (1990).
[2] STONEKING, M.R. et al., Phys. of Plasmas **5** (1998) 1004.
[3] CAPELLO, S., BISKAMP, D., Nucl. Fusion **36** (1996) 571.
[4] CAPELLO, S., PACCAGNELLA, R., Phys. Fluids B **4** (1992) 611.
[5] FINN, J. et al., Phys. Fluids B **4** (1992) 1262.
[6] MARTIN, P. et al., this conference IAEA-CN-94/EX/C1-2.
[7] SARFF, J.S. et al., Phys. Rev. Lett. **72** (1994) 3670.

[8] BARTIROMO, R. et al., Phys. Rev. Lett. **82** (1999) 1492.
[9] CHAPMAN, B. et al., Phys. Rev. Lett. **87** (2001) 205001.
[10] SAKAKITA, H. et al., this conference IAEA-CN-94/EX/P2-07.
[11] DEXTER, R.N. et al., Fusion Technol. (1991) 131.
[12] CHAPMAN, B. et al., Phys. of Plasmas **9** (2002) 2061.
[13] FIKSEL, G. et al., this conference IAEA-CN-94/EX/C4-6
[14] ANDERSON, J., Ph.D. dissertation, University of Wisconsin-Madison (2001).
[15] BROWER, D.L. et al., this conference IAEA-CN-94/EX/P4-01.
[16] CRAIG, D.J. et al., Rev. Sci. Instrum. **72** (2001) 1008.
[17] ITER Physics Expert Groups on Confinement and Transport and Confinement Modelling and Database, Nucl. Fusion **39** (1999) 2175.
[18] O'CONNELL, R. et al, "Transition from stochastic magnetic to electrostatic-like transport in the RFP." submitted to Phys. Rev. Lett. (2002).
[19] HARVEY, R.A., GA report GA-A20978 (1992).
[20] BIEWER, T.M. et al., "Electron heat transport measured in a stochastic magnetic field," submitted to Phys. Rev. Lett. (2002).
[21] SCHNACK, D.D. et al., Jou. Comp. Phys. **70** (1987) 330.
[22] RECHESTER, A., ROSENBLUTH, M., Phys. Rev. Lett. **40** (1978) 38.
[23] FOREST, C.B. et al., Phys. of Plasmas **7** (2000) 1352.
[24] BEVIR, M.K. et al., Phys. Fluids **28** (1985) 1826.
[25] SCHOENBERG, K.F. et al., Phys. Fluids **27** (1984) 2881.
[26] EBRAHIMI, F. et al, "The three-dimensional MHD dynamics of AC helicity injection in the Reversed Field Pinch," submitted to Phys. of Plasmas (2002).
[27] ABDRASHITOV, G.F. et al., Rev. Sci. Instrum. **72** (2001) 594.